Composites Part B 157 (2019) 173–181

Contents lists available at ScienceDirect

Composites Part B

journal homepage: www.elsevier.com/locate/compositesb

Effect of concrete creep on dynamic stability behavior of slender concrete-filled steel tubular column

Y.Q. Huang[a], J.Y. Fu[a,*], A.R. Liu[a], Y.L. Pi[a,b], D. Wu[a,b], W. Gao[a]

[a] Centre for Engineering Structure Disaster Prevention and Control, Guangzhou University, Guangzhou 510006, China
[b] Centre for Infrastructure Engineering and Safety (CIES), School of Civil and Environmental Engineering, The University of New South Wales Sydney, NSW 2052, Australia

ARTICLE INFO

Keywords:
Slender concrete-filled steel tube column
Dynamic stability
Time analysis
Age-adjusted effective modulus method
Bolotin's method

ABSTRACT

An analytical procedure for dynamic stability of CFST column accounting for the creep of concrete core is proposed. The long-term effect of creep of concrete core is formulated based on the creep model by the ACI 209 committee and the age-adjusted effective modulus method (AEMM). The equations of boundary frequencies accounting for the effects of concrete creep are derived by the Bolotin's theory and solved as a quadratic eigenvalue problem. The effectiveness of the proposed method and the characteristics of time-varying distribution of instability regions are numerically surveyed. It is shown that the CFST column becomes dynamically unstable even when the sum of the sustained static load and the amplitude of the dynamic excitation is much lower than the static instability load. It is also found that due to the time effects of concrete creep under the sustained static load, the same excitation, that cannot induce dynamic instability in the early stage of sustained loading, can induce the dynamic instability in a few days later. The critical amplitude and frequency of the dynamic excitation can decrease by 6% and 3% in 5 days, and 11% and 6% in 100 days.

1. Introduction

Steel hollow sections are very efficient in resisting compression forces, and filling these sections with concrete greatly enhances the load-carrying capacity [1,2]. The concrete-filled steel tubular (CFST) structure possesses many mechanic benefits, such as high strength and fire resistances, favorable ductility and large energy absorption capacities, so the CFST members are widely used in modern structures [3]. Moreover, with the advancement in the strength resistance and construction techniques of CFST column, slender CFST columns are frequently adopted to support the roofs of industrial plants, the decks of railways and the floors of multistory buildings [4].

It is known when a slender column is subject to an axial compression, it could fail owing to lateral instability [5]. The instability of slender CFST columns under axial static compression has been experimentally and numerically studied by many researchers [4,6–8]. These studies have shown that slender CFST columns are prone to global buckling under static loading. In addition to the static loading, the service loads of slender CFST members also involve the dynamic loading. For example, the slender CFST piers in modern bridges are subject to the dynamic vehicle loading, and the high CFST pillars supporting large span roofs are loaded by dynamic wind loading. The behavior of CFST columns subjected to cycles of compressive loading has also been reported by many researchers [9–11]. Under a sustained centric axial static load, the concrete core of a CFST column creeps with the time and the creep of the concrete core may change the lateral stiffness and the lateral natural frequency of the CFST column significantly. If the column under the sustained load is further excited by an axial dynamic excitation at some stage, the column may suddenly lose its stability laterally due to dynamic resonance when certain relationships between the frequency of excitation and the natural frequency of the column are satisfied and the amplitudes of the excitation are sufficiently high. Because the creep of the concrete core develops with the time and changes the lateral natural frequency, the relationships between the frequency of the excitation and the natural frequency of the column and the required amplitude of the excitation inducing the dynamic instability of the CFST column may change greatly with the time. Such dynamic instability may occur even when the sum of the amplitude of the excitation and the sustained static load is much smaller than the static instability load of the column.

Meanwhile, the engineering structures are commonly subject to sustained static loads and sudden dynamic excitations [12,13]. Since the mechanical property of the concrete core is time-dependent due to creep when it is under a sustained load, the dynamic stability of a CFST

* Corresponding author.
E-mail address: jiyangfu@gzhu.edu.cn (J.Y. Fu).

https://doi.org/10.1016/j.compositesb.2018.08.117
Received 1 July 2018; Accepted 23 August 2018
Available online 27 August 2018

column under dynamic excitation would be affected by the loading time difference between the first static loading and the dynamic excitation. However, there is no knowledge about how the creep of the concrete core influences the dynamic stability of a CFST column available in the literature hitherto. To ensure that CFST columns under sustained static loads and sudden dynamic excitations do not suddenly lost their stability, it is much needed to investigate the effects of the creep of the concrete core on the dynamic stability of CFST columns.

This study, therefore, is devoted to establishing an analytical procedure for the time-dependent dynamic stability analysis of slender CFST columns accounting for the creep of the concrete core. The column under a sustained static load and suddenly subjected to a dynamic excitation is considered. The age-adjusted effective modulus method (AEMM) is used to describe the effect of the creep on the effective modulus of the concrete and the time-dependent model of concrete creep of the ACI committee 209 [14] is adopted in the investigation. Based on these, the differential equation of lateral motion of the CFST column under the dynamic excitation is derived. The equations of boundary frequencies are then established by the Bolotin's method and they are solved to determine the boundaries of regions of dynamic instability. Finally, the effectiveness of the proposed method and the characteristics of time-dependent dynamic stability of CFST columns accounting for the creep of the concrete core are discussed by elaborate numerical examinations.

2. Creep of concrete core under sustained static load

The aging property of the concrete was firstly noticed about 110 years ago, and a large amount of literature have been concentrated on this subject, such as the books by Bazant [5], Neville [15] and Gilbert [16]. The final total strain of the concrete at time infinity could be several times the initially instantaneous strain, so the analysis overlooking the time effect might extraordinarily underestimate the load effect in the concrete or concrete-composite structures [17–19]. The gradual development of strains in the sustained loaded concrete is due to the creep and shrinkage of the concrete [16]. The creep and shrinkage strains of CFST columns with various cross-sectional shapes and concrete types were widely tested [20–22] and numerically computed [23–25]. It was found that the shrinkage of the concrete in CFST columns is very small and negligible owing to the prevention of moisture egress in a seated environment [25,26].

This study assumes that the CFST column is under a centric axial sustained static load for some time and then is suddenly subjected to a centric axial dynamic excitation for a short period. Under the sustained axial load, the effective modulus of the concrete changes with the time due to the creep of the concrete core. The age-adjusted effective modulus method [27] is adopted in this investigation. According to the method, the effective modulus of concrete E_{ec} at the time t_1 is given by

$$E_{ec}(t_1, \tau_0) = \frac{E_c(\tau_0)}{1 + \chi(t_1, \tau_0)\varphi(t_1, \tau_0)} \tag{1}$$

where $E_c(\tau_0)$ represents the elastic modulus of concrete at the time τ_0 of first loading; $\varphi(t_1,\tau_0)$ is the creep coefficient and $\chi(t_1,\tau_0)$ is the aging coefficient.

The time-related creep coefficient $\varphi(t_1,\tau_0)$ can be determined according to the long-term model proposed by the ACI committee 209 [14].

$$\varphi(t_1, \tau_0) = \frac{(t_1 - \tau_0)^{0.6}}{10 + (t_1 - \tau_0)^{0.6}}\varphi^*(\tau_0) \tag{2}$$

where $(t_1$-$\tau_0)$ denotes the duration of loading (in days); $\varphi^*(\tau_0)$ is the final creep coefficient. According to the existing creep test results [21,28], the final creep coefficient $\varphi^* = 2.29$ is used here.

Additionally, the aging coefficient $\chi\ (t_1,\tau_0)$ can be computed by the empirical expression [16,29].

$$\chi\left(t_1, \tau_0\right) = 1 - \frac{(1 - \chi^*)(t_1 - \tau_0)}{20 + t_1 - \tau_0} \tag{3}$$

where χ^* is the final aging coefficient

$$\chi^* = \frac{k_1\tau_0}{k_2 + \tau_0} \tag{4}$$

with

$$k_1 = 0.78 + 0.4e^{-1.33\varphi^*(\tau_0)} \text{ and } k_2 = 0.16 + 0.8e^{-1.33\varphi^*(\tau_0)} \tag{5}$$

Therefore, for a CFST column under sustained static loading from the time τ_0, when the column is dynamically excited at the time t_1, the effective modulus of concrete at time t_1 can be computed by Eqs. (1)–(5) for the dynamic stability analysis of the CFST column under a dynamic excitation starting at the time t_1.

3. Dynamic stability analysis accounting for creep of concrete core

3.1. Governing equation of dynamic stability

A simply-supported CFST column is initially subjected to a sustained axial concentric static load P_0 from the time τ_0 and then subjected to an additional dynamical excitation from a time t_1 ($t_1 > \tau_0$), as shown in Fig. 1. Without loss of generality, the dynamic excitation is considered as a harmonic type excitation $P(t) = P_0 + P_t \cos \theta t$ with the period $T = 2\pi/\theta$, where P_0 is the sustained static load, and P_t and θ denote the amplitude and circular frequency of dynamic excitations.

For a straight column subject to an axial excitation, it would vibrate in the axial direction. However, when certain relationships between the frequency and amplitude of the excitation and the lateral natural frequency of the column are satisfied, the column may suddenly vibrate laterally and lose its stability in a dynamic resonance instability mode [30–34]. The initial and deformed configurations of CFST column during dynamic instability is shown in Fig. 1a. The length of column is L, and the lateral displacement of column is represented by $u(x,t)$, where t is the time and x is the coordinate along the length of column. The cross section of column consisted of a steel tube and a concrete core is shown in Fig. 1b.

Forces acting on the infinitesimal element dx in the deformed position of the column are shown in Fig. 1c. These forces include the inertia force $m_e\partial^2u/\partial t^2$ and the viscous damping force $c(x)\partial u/\partial t$, where m_e is the equivalent mass per unit length of the column and $c(x)$ is a damping constant; the axial force N, the shear force V and the moment M at the bottom of the element; and the axial force $N+(\partial N/\partial x)\mathrm{d}x$, the shear force $V+(\partial V/\partial x)\mathrm{d}x$, and the moment $M+(\partial M/\partial x)\mathrm{d}x$ on the top of the element. The inertial moment caused by the angular acceleration of the element is neglected.

The following assumptions are adopted for the dynamic stability analysis of CFST columns [28,35,36]: (1) the size of the cross section of the CFST column is much smaller than the length of the column such that the column is sufficiently slender; (2) oscillation of CFST column is small and the deformation is linearly elastic, which satisfies the Euler-Bernoulli hypothesis on that the cross section remains plane and perpendicular to the column axis during deformation; (3) the concrete core and the steel tube of the CFST column are fully bonded; and (4) the flexural stiffness of the CFST column is regarded as constant along the CFST column. Because the axial rigidity of the CFST column is much higher than its lateral rigidity, the influence of the axial vibration on the lateral vibration is negligible and the internal axial force is equal to the sum of the sustained static load and the external axial excitation.

Based on the assumptions, considering the forces acting on the infinitesimal element shown in Fig. 1, the equation of motion for the column be derived as

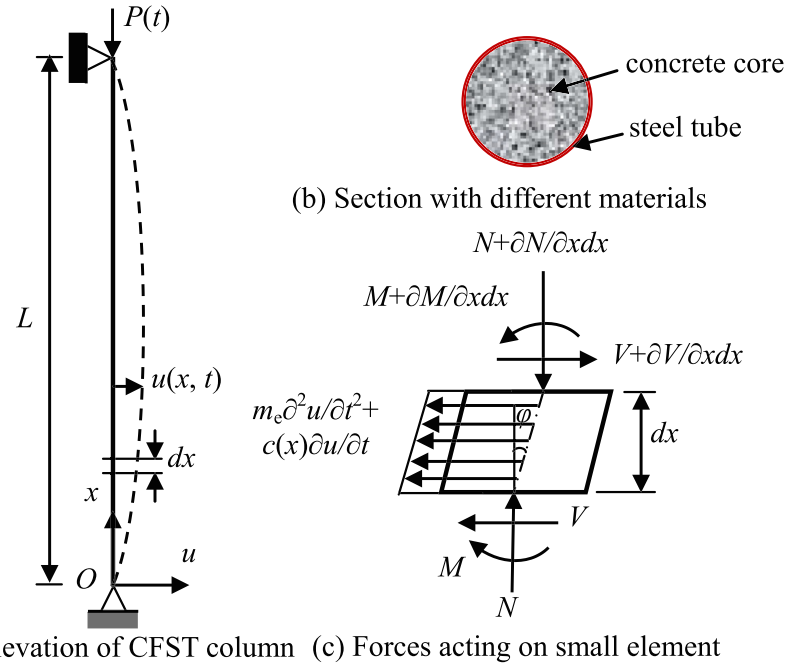

Fig. 1. Lateral resonance of a CFST column.

$$\frac{\partial V(x,t)}{\partial x} - m_e \frac{\partial^2 u(x,t)}{\partial t^2} - c(x)\frac{\partial u(x,t)}{\partial t} = 0 \tag{6}$$

and the equation of equilibrium of internal forces can also be derived as

$$V(x,t) + N(x,t)\phi - \frac{\partial M(x,t)}{\partial x} = 0 \tag{7}$$

where $m_e = \rho_s A_s + \rho_c A_c$, ρ_s and ρ_c denote the densities of the steel tube and the concrete core, respectively, and A_s and A_c denote the cross-sectional areas of the steel tube and the concrete core, respectively; the small angle φ can be calculated by $\varphi = \partial u/\partial x$.

As the angle φ is small, the curvature of the column can be calculated by Ref. [37].

$$\frac{1}{\kappa} = \frac{\partial^2 u/\partial x^2}{[1 + (\partial u/\partial x)^2]^{3/2}} \approx \frac{\partial^2 u}{\partial x^2} \tag{8}$$

where κ is the radius of curvature.

Based on the first two assumptions, for the initially straight column of a uniform cross section, the normal strain ε_x in the x-direction across the section can be expressed as

$$\varepsilon_x = -\frac{1}{\kappa}y = -\frac{\partial^2 u}{\partial x^2}y \tag{9}$$

where y is the distance between the location point of ε_x and the neutral surface of the column.

According to the third assumption that the concrete core is fully bonded with the steel tube, the deformations of the steel tube and the concrete core must be compatible with each other, so the steel tube and the concrete core have the same normal strain at their interface and thus the same radius of curvature [38]. Therefore, both the normal strains at the cross sections of the steel tube and the concrete core can be calculated by Eq. (9). Moreover, the stress of the steel tube is different from that of the concrete core at the interface due to the fact that they have different Young's moduli. The stresses are computed by Ref. [39].

$$\sigma_s = E_s \varepsilon_{x,s} = E_s\left(-\frac{\partial^2 u}{\partial x^2}y_s\right) \tag{10}$$

$$\sigma_c = E_{ec} \varepsilon_{x,c} = E_{ec}\left(-\frac{\partial^2 u}{\partial x^2}y_c\right) \tag{11}$$

where σ_s and σ_c denote the normal stresses on the cross section of the steel tube and the concrete core, respectively; y_s and y_c correspond to the values of y of the steel tube and the concrete core, respectively; E_s denotes the elastic modulus of steel; and E_{ec} denotes the age-adjusted effective modulus of concrete, which is computed by Eqs. (1)–(5).

Thus, the moment M at the cross-section of CFST column due to the normal stresses can be expressed as

$$M = -\int_{A_s} y_s \sigma_s dA_s - \int_{A_c} y_c \sigma_c dA_c = -(E_s I_s + E_{ec}(t_1) I_c)\frac{\partial^2 u}{\partial x^2} \tag{12}$$

where $E_s I_s + E_{ec}(t_1) I_c$ denotes the effective lateral stiffness of the CFST column and t_1 is the time when the periodic excitation is acted; I_s and I_c are the second moments of area of the cross section of the steel tube and the concrete core, respectively.

Substituting Eq. (12) into Eq. (7) gives the shear force V as

$$V(x,t) = -N(x,t)\frac{\partial u(x,t)}{\partial x} - \frac{\partial}{\partial x}\left[(E_s I_s + E_{ec}(t_1) I_c)\frac{\partial^2 u(x,t)}{\partial x^2}\right] \tag{13}$$

By further differentiating Eq. (13) with respect to x and substituting into Eq. (6), the time-dependent governing equation for the lateral vibration of the CFST column under an axial load $P(t)$ can be obtained as

$$m_e \frac{\partial^2 u(x,t)}{\partial t^2} + c(x)\frac{\partial u(x,t)}{\partial t} + \quad + \quad = 0 \tag{14}$$

Based on the above fourth assumption, the effective stiffness $E_s I_s + E_{ec}(t_1) I_c$ is independent of x and the axial force $N(x,t) = P(t)$ and so Eq. (14) can be simplified as

$$m_e \frac{\partial^2 u(x,t)}{\partial t^2} + c(x)\frac{\partial u(x,t)}{\partial t} + (E_s I_s + E_{ec}(t_1) I_c)\frac{\partial^4 u(x,t)}{\partial x^4} + P(t)\frac{\partial^2 u(x,t)}{\partial x^2} = 0 \tag{15}$$

In analyzing the structural dynamic stability problem, the dynamic response is generally expanded with respect to the free vibration forms [30,40,41]. Thus, the lateral dynamic response $u(x,t)$ can be expressed as [42].

$$u(x,\ t) = \sum_{n=1}^{\infty} y_n(t)\sin\frac{n\pi x}{L} \tag{16}$$

where $y_n(t)$ denotes the n-th modal response of the column; and sin $(n\pi x/L)$ denotes the n-th mode shape of a simply-supported column.

By substituting Eq. (16) into Eq. (15), it can be obtained that

$$\sum_{n=1}^{\infty}\left[\begin{array}{l} m_e\frac{d^2y_n(t)}{dt^2} + c(x)\frac{dy_n(t)}{dt} + \\ (E_sI_s + E_{ec}(t_1)I_c)\left(\frac{n\pi}{L}\right)^4 y_n(t) - P(t)\left(\frac{n\pi}{L}\right)^2 y_n(t)\end{array}\right]\sin\frac{n\pi x}{L} = 0 \tag{17}$$

It is clear that for Eq. (16) to satisfy Eq. (15), the quantity in the square bracket of Eq. (17) should vanish at any time t as

$$\begin{array}{l} m_e\frac{d^2y_n(t)}{dt^2} + c(x)\frac{dy_n(t)}{dt} + \\ \quad (E_sI_s + E_{ec}(t_1)I_c)\left(\frac{n\pi}{L}\right)^4 y_n(t) - P(t)\left(\frac{n\pi}{L}\right)^2 y_n(t) = 0 \quad (n = 1,2,\cdots,\infty)\end{array} \tag{18}$$

Eq. (18) can further be written as

$$\frac{d^2y_n(t)}{dt^2} + \frac{c(x)}{m_e}\frac{dy_n(t)}{dt} + \omega_n^2(t_1)\left[1 - \frac{P(t)}{P_{cr,n}(t)}\right]y_n(t) = 0 \quad (n = 1,2,\cdots,\infty) \tag{19}$$

where

$$\omega_n(t_1) = \left(\frac{n\pi}{L}\right)^2\sqrt{\frac{E_sI_s + E_{ec}(t_1)I_c}{m_e}} \tag{20}$$

and

$$P_{cr,n}(t_1) = (E_sI_s + E_{ec}(t_1)I_c)\left(\frac{n\pi}{L}\right)^2 \tag{21}$$

denote the n-th natural frequency of free vibration of the unloaded column at the time t_1 of being subjected to the periodic excitation and the n-th Euler buckling load of the column.

When a CFST column is only statically loaded by the central axial load P_0, it would lose its stability when P_0 reaches the static critical load $P_{cr,\ n}(t_1)$ of the column. However, when the CFST column under a central axial static load P_0 much smaller than $P_{cr,\ n}(t_1)$ can dynamically lose its stability when it is excited by an central axial periodic load. It is shown in Eqs. (19)–(21) that the time effect of the creep of the concrete core is mainly manifested in the structural frequency $\omega_n(t_1)$ and Euler load $P_{cr,\ n}(t_1)$.

Considering $P(t) = P_0 + P_t\cos\theta t$, Eq. (19) yields

$$\begin{array}{l}\frac{d^2y_n(t)}{dt^2} + \frac{c(x)}{m_e}\frac{dy_n(t)}{dt} + \Omega_n^2(t_1)[1 - 2\mu_n(t_1)\cos\theta t]y_n(t) \\ \quad = 0 \quad (n = 1,2,\cdots,\infty)\end{array} \tag{22}$$

where

$$\Omega_n(t_1) = \omega_n(t_1)\sqrt{1 - \frac{P_0}{P_{cr,n}(t_1)}} \tag{23}$$

denotes the n-th frequency of the column under the load P_0, and

$$\mu_n(t_1) = \frac{P_t}{2(P_{cr,n}(t_1) - P_0)} \tag{24}$$

is the excitation parameter.

Eq. (22) is the differential equation for the dynamic stability analysis of CFST column subject to a parametric excitation accounting for the effects of creep of the concrete core. According to Eq. (22), each mode of a column affects the dynamic stability of the column independently. That is, the dynamic stability of a CFST column can be represented by the dynamic stability in any mode of the column. Consequently, the index n in Eq. (22) can be dropped and Eq. (22) is then expressed as

$$\frac{d^2y(t)}{dt^2} + 2\xi\omega(t)\frac{dy(t)}{dt} + \Omega^2(t_1)[1 - 2\mu(t_1)\cos\theta t]y(t) = 0 \tag{25}$$

where ξ is the modal damping coefficient defined by $2\xi\omega = c/m_e$.

3.2. Time-dependent boundaries of regions of dynamic instability

As a Mathieu-Hill type equation, the convergence of solutions of Eq. (25) is closely related to the characteristic roots of Eq. (25). The real characteristic roots yield regions of unbounded solutions, and the complex characteristic roots produce the region of bounded solutions. Moreover, the multiple characteristic roots correspond to the boundaries between the instability regions and the stability regions [30]. Because the multiple roots denote that Eq. (25) has the periodic solutions with the period T or 2T ($T = 2\pi/\theta$) of the column, the issue of computing the boundaries of regions of dynamic instability is reduced to finding the conditions under which Eq. (25) has periodic solutions [43,44].

Thus, a periodic solution of Eq. (25) with the period 2T can be expressed as

$$y(t) = \sum_{k=1,3,5}^{\infty}\left(a_k\sin\frac{k\theta t}{2} + b_k\cos\frac{k\theta t}{2}\right) \tag{26}$$

where a_k and b_k are coefficients independent of time.

By substituting Eq. (26) into Eq. (25) and comparing the coefficients of identical terms of $\sin(k\theta t/2)$ and $\cos(k\theta t/2)$, it yields

$$\mathbf{A}_{2T}(t_1)\mathbf{x}_{2T} = \mathbf{0} \tag{27}$$

where

$$\mathbf{x}_{2T} = \{\cdots, a_5, a_3, a_1, b_1, b_3, b_5, \cdots\}^T \tag{28}$$

$$\mathbf{A}_{2T}(t_1) = \begin{bmatrix}\mathbf{A}_{2T,11}(t_1) & \mathbf{A}_{2T,12}(t_1)\\ \mathbf{A}_{2T,21}(t_1) & \mathbf{A}_{2T,22}(t_1)\end{bmatrix} \tag{29}$$

with

$$\mathbf{A}_{2T,11}(t_1) = \begin{bmatrix}\cdots & \cdots & \cdots & \cdots\\ \cdots & 1 - \frac{25\theta^2}{4\Omega^2(t_1)} & -\mu(t_1) & 0\\ \cdots & -\mu(t_1) & 1 - \frac{9\theta^2}{4\Omega^2(t_1)} & -\mu(t_1)\\ \cdots & 0 & -\mu(t_1) & 1 + \mu(t_1) - \frac{\theta^2}{4\Omega^2(t_1)}\end{bmatrix} \tag{30a}$$

$$\mathbf{A}_{2T,12}(t_1) = \begin{bmatrix}\cdots & \cdots & \cdots & \cdots\\ 0 & 0 & -2\xi\frac{5\theta}{2\Omega(t_1)} & \cdots\\ 0 & -2\xi\frac{3\theta}{2\Omega(t_1)} & 0 & \cdots\\ -2\xi\frac{\theta}{2\Omega(t_1)} & 0 & 0 & \cdots\end{bmatrix} \tag{30b}$$

$$\mathbf{A}_{2T,21}(t_1) = \begin{bmatrix}\cdots & 0 & 0 & 2\xi\frac{\theta}{2\Omega(t_1)}\\ \cdots & 0 & 2\xi\frac{3\theta}{2\Omega(t_1)} & 0\\ \cdots & 2\xi\frac{5\theta}{2\Omega(t_1)} & 0 & 0\\ \cdots & \cdots & \cdots & \cdots\end{bmatrix} \tag{30c}$$

and

$$\mathbf{A}_{2T,22}(t_1) = \begin{bmatrix}1 - \mu(t_1) - \frac{\theta^2}{4\Omega^2(t_1)} & -\mu(t_1) & 0 & \cdots\\ -\mu(t_1) & 1 - \frac{9\theta^2}{4\Omega^2(t_1)} & -\mu(t_1) & \cdots\\ 0 & -\mu(t_1) & 1 - \frac{25\theta^2}{4\Omega^2(t_1)} & \cdots\\ \cdots & \cdots & \cdots & \cdots\end{bmatrix} \tag{30d}$$

Similarly, the periodic solution of Eq. (25) with the period T has the form

$$y(t) = \frac{1}{2}b_0 + \sum_{k=2,4,6}^{\infty}\left(a_k \sin\frac{k\theta t}{2} + b_k \cos\frac{k\theta t}{2}\right) \tag{31}$$

Substituting Eq. (31) into Eq. (25) leads to

$$\mathbf{A}_T(t_1)\mathbf{x}_T = \mathbf{0} \tag{32}$$

where

$$\mathbf{x}_T = \{\cdots, a_6, a_4, a_2, b_0, b_2, b_4, \cdots\}^T \tag{33}$$

and

$$\mathbf{A}_T(t_1) = \begin{bmatrix} \mathbf{A}_{T,11}(t_1) & \mathbf{A}_{T,12}(t_1) \\ \mathbf{A}_{T,21}(t_1) & \mathbf{A}_{T,22}(t_1) \end{bmatrix} \tag{34}$$

with

$$\mathbf{A}_{T,11}(t_1) = \begin{bmatrix} \cdots & \cdots & \cdots & \cdots \\ \cdots & 1-\frac{9\theta^2}{\Omega^2(t_1)} & -\mu(t_1) & 0 \\ \cdots & -\mu(t_1) & 1-\frac{4\theta^2}{\Omega^2(t_1)} & -\mu(t_1) \\ \cdots & 0 & -\mu(t_1) & 1-\frac{\theta^2}{\Omega^2(t_1)} \end{bmatrix} \tag{35a}$$

$$\mathbf{A}_{T,12}(t_1) = \begin{bmatrix} \cdots & \cdots & \cdots & \cdots \\ 0 & 0 & 0 & \cdots \\ 0 & 0 & -2\xi\frac{2\theta}{\Omega(t_1)} & \cdots \\ 0 & -2\xi\frac{\theta}{\Omega(t_1)} & 0 & \cdots \end{bmatrix} \tag{35b}$$

$$\mathbf{A}_{T,21}(t_1) = \begin{bmatrix} \cdots & 0 & 0 & 0 \\ \cdots & 0 & 0 & 2\xi\frac{\theta}{\Omega(t_1)} \\ \cdots & 0 & 2\xi\frac{2\theta}{\Omega(t_1)} & 0 \\ \cdots & \cdots & \cdots & \cdots \end{bmatrix} \tag{35c}$$

and

$$\mathbf{A}_{T,22}(t_1) = \begin{bmatrix} 1 & -\mu(t_1) & 0 & \cdots \\ -2\mu(t_1) & 1-\frac{\theta^2}{\Omega^2(t_1)} & -\mu(t_1) & \cdots \\ 0 & -\mu(t_1) & 1-\frac{4\theta^2}{\Omega^2(t_1)} & \cdots \\ \cdots & \cdots & \cdots & \cdots \end{bmatrix} \tag{35d}$$

Eqs. (27) and (32) are the systems of linear homogeneous equations and so the non-trivial solutions exist only if the determinants of their coefficient matrices vanish

$$\det(\mathbf{A}_{2T}(t_1)) = 0 \tag{36}$$

and

$$\det(\mathbf{A}_T(t_1)) = 0 \tag{37}$$

Eqs. (36) and (37) can be solved in a quadratic form as [33,34,45].

$$\det\left[\mathbf{A}_0(t_1) - \frac{\theta}{2\Omega}\mathbf{A}_1 - \left(\frac{\theta}{2\Omega}\right)^2\mathbf{A}_2\right] = 0 \tag{38}$$

where the matrices $\mathbf{A}_0$, $\mathbf{A}_1$ and $\mathbf{A}_2$ corresponding to Eq. (36) are

$$\mathbf{A}_0(t_1) = \begin{bmatrix} \cdots & \cdots & \cdots & \cdots & \cdots & \cdots \\ \cdots & 1 & -\mu(t_1) & 0 & 0 & \cdots \\ \cdots & -\mu(t_1) & 1+\mu(t_1) & 0 & 0 & \cdots \\ \cdots & 0 & 0 & 1-\mu(t_1) & -\mu(t_1) & \cdots \\ \cdots & 0 & 0 & -\mu(t_1) & 1 & \cdots \\ \cdots & \cdots & \cdots & \cdots & \cdots & \cdots \end{bmatrix} \tag{39a}$$

$$\mathbf{A}_1 = \begin{bmatrix} \cdots & \cdots & \cdots & \cdots & \cdots & \cdots \\ \cdots & 0 & 0 & 0 & 6\xi & \cdots \\ \cdots & 0 & 0 & 2\xi & 0 & \cdots \\ \cdots & 0 & -2\xi & 0 & 0 & \cdots \\ \cdots & -6\xi & 0 & 0 & 0 & \cdots \\ \cdots & \cdots & \cdots & \cdots & \cdots & \cdots \end{bmatrix}, \text{and } \mathbf{A}_2 = \begin{bmatrix} \cdots & \cdots & \cdots & \cdots & \cdots & \cdots \\ \cdots & 9 & 0 & 0 & 0 & \cdots \\ \cdots & 0 & 1 & 0 & 0 & \cdots \\ \cdots & 0 & 0 & 1 & 0 & \cdots \\ \cdots & 0 & 0 & 0 & 9 & \cdots \\ \cdots & \cdots & \cdots & \cdots & \cdots & \cdots \end{bmatrix} \tag{39b}$$

and those corresponding to Eq. (37) are

$$\mathbf{A}_0(t_1) = \begin{bmatrix} \cdots & \cdots & \cdots & \cdots & \cdots & \cdots \\ \cdots & 1 & -\mu(t_1) & 0 & 0 & \cdots \\ \cdots & -\mu(t_1) & 1 & 0 & 0 & \cdots \\ \cdots & 0 & 0 & 1 & -\mu(t_1) & \cdots \\ \cdots & 0 & 0 & -2\mu(t_1) & 1 & \cdots \\ \cdots & \cdots & \cdots & \cdots & \cdots & \cdots \end{bmatrix} \tag{40a}$$

$$\mathbf{A}_1 = \begin{bmatrix} \cdots & \cdots & \cdots & \cdots & \cdots & \cdots \\ \cdots & 0 & 0 & 0 & 0 & \cdots \\ \cdots & 0 & 0 & 0 & 4\xi & \cdots \\ \cdots & 0 & 0 & 0 & 0 & \cdots \\ \cdots & 0 & -4\xi & 0 & 0 & \cdots \\ \cdots & \cdots & \cdots & \cdots & \cdots & \cdots \end{bmatrix}, \text{and } \mathbf{A}_2 = \begin{bmatrix} \cdots & \cdots & \cdots & \cdots & \cdots & \cdots \\ \cdots & 16 & 0 & 0 & 0 & \cdots \\ \cdots & 0 & 4 & 0 & 0 & \cdots \\ \cdots & 0 & 0 & 0 & 0 & \cdots \\ \cdots & 0 & 0 & 0 & 1 & \cdots \\ \cdots & \cdots & \cdots & \cdots & \cdots & \cdots \end{bmatrix} \tag{40b}$$

When the damping coefficient ξ and the loading time difference between the static load and the periodic excitation are given, the critical frequency ratio $\theta/2\Omega(t_1)$ corresponding to each excitation parameter $\mu(t_1)$ can be determined by solving the equation of boundary frequencies given by Eq. (38). The odd and even regions of dynamic instability corresponding to Eqs. (39) and (40) can then be obtained respectively and displayed on the parametric plane (θ, P_t) under a given static load P_0.

4. Numerical investigations

In order to verify the effectiveness of the proposed method and explore the effects of the creep of the concrete core on the dynamic stability of CFST columns, a CFST column with the slenderness ratio of 160 is investigated in this section. The length of the CFST column is 4.0 m, while the outer diameter and thickness of the steel tube are 100 mm and 5 mm, respectively. The modal damping coefficient for the CFST column proposed in Ref. [45] is adopted as $\xi = 0.02$. Other related material parameters of steel and concrete are shown in Table 1.

By the proposed method, all the odd and even regions of dynamic instability of the CFST column at the time t_1 can be obtained. Meanwhile, since the first region of dynamic instability is the principal one with great significance [30,34], it is mainly investigated in this work.

4.1. Numerical verification on the instability region

The first or principal region of dynamic instability of the CFST column at $t_1 = \tau_0 = 15$ days is shown in Fig. 2a for $P_0 = 133$ kN. The abscissa $\theta/2\omega_1$ denotes the ratio of the excitation frequency to the first natural frequency of column at time t_1. The red-shaded area represents the principal region of dynamic instability. Fig. 2a shows that the CFST column would become dynamically unstable when $\theta/2\omega_1$ is in the vicinity of 0.7. Moreover, when a parametric point ($\theta/2\omega_1$, P_t) corresponding to a specific CFST column and an excitation locates inside the region of instability, the column would become dynamically unstable

Table 1
Material parameters of the CFST column.

Steel		Concrete			
ρ_s (kg/m^3)	E_s (GPa)	ρ_c (kg/m^3)	τ_0 (day)	$E_c(\tau_0)$ (GPa)	$\varphi^*(\tau_0)$
7850	202	2400	15	27.6	2.29

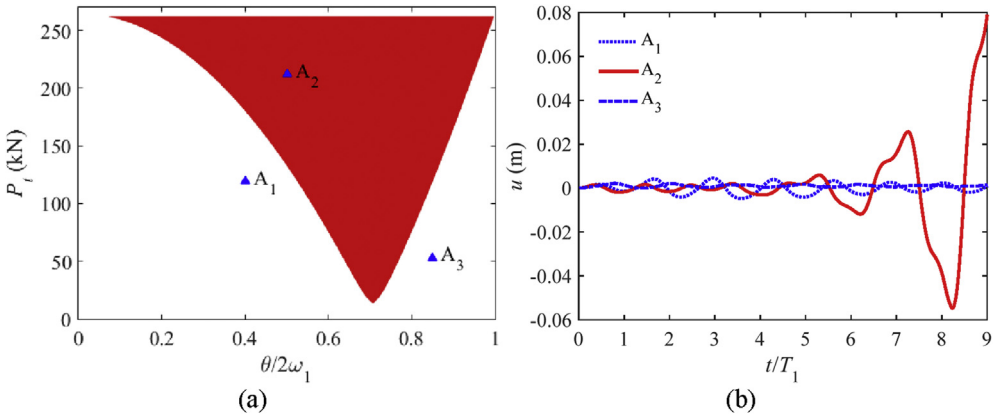

Fig. 2. Comparison of dynamic stability between instability region and dynamic responses (a) Principal region of instability; (b) Dynamic response.

under the excitation, i.e. its dynamic response could be divergent under the excitation. On the other hand, if the parametric point is situated outside the instability region, the column should vibrate stably around its equilibrium position under the excitation. Therefore, the validity and accuracy of the boundaries separating the instability regions from the stability regions are very crucial for arriving at the correct conclusion on the dynamic stability of a CFST column.

In order to verify the validity of the boundaries, three parametric points A_1 to A_3 are randomly selected around the boundary of the principal instability region, as shown in Fig. 2a, and their corresponding dynamic responses of the CFST column are computed by a finite element (FE) model of ANSYS. The FE model of CFST column, which is simulated by a 2-D elastic element BEAM3, possesses the geometric, material and boundary condition properties identical to those in the dynamic instability analysis by the proposed analytical method. The dynamic responses of the CFST column are shown in Fig. 2b, where the abscissa t is non-dimensionalized by the first natural period T_1 of the CFST column and the ordinate denotes the response $u(L/2,t)$ at the middle of the column. It can be seen from Fig. 2 that the dynamic response corresponding to point A_2 diverges with time while the dynamic responses of other two points A_1 and A_3 are steady and stable with time. This agrees with the conclusion from the region of dynamic instability that the point A_2 locates inside the instability region while other points are outside the instability region. Thus, the results of the proposed method agree with the FE results excellently.

4.2. Time-dependent characteristics of dynamic instability

4.2.1. Time-related parameters

According to Eq. (2), the creep coefficient $\varphi(t_1,\tau_0)$ increases from 0 (at τ_0 = 15 days) to 1.97 (at t_1 = 1000 days), which is 86% of its final value 2.29 (Fig. 3). The day rate of change of $\varphi(t_1,\tau_0)$, defined as $[\varphi(t_i,\tau_0)-\varphi(t_i\text{-}1,\tau_0)]/\varphi(t_i\text{-}1,\tau_0)$, possess a maximum value of about 45% at the beginning of loading and becomes less than 0.01% after about 880 days.

From Eq. (3), the aging coefficient $\chi(t,\tau_0)$ decreases from 1.0 (at τ_0 = 15 days) to 0.793 (at t_1 = 1000 days), which is 99.5% of the final aging coefficient χ^* = 0.789 (Fig. 3). The absolute day rate of change of χ is about 1% at the beginning of loading and becomes less than 0.01% after about 210 days.

Owing to the variations of φ and χ with time, the effective modulus E_{ec} of the concrete decreases from 27.6 GPa to 10.76 GPa in about 1000 days according to Eq. (1), which drops by about 61% (Fig. 4). The absolute day rate of change of E_{ec} has its maximum of 17% at the beginning of sustained loading and goes below 0.01% after about 600 days. Accordingly, the effective lateral stiffness (E_sI_s + $E_{ec}I_c$) of the CFST column investigated in this paper decreases by 12.6% in about 1000 days, and its absolute day rate of change goes under 0.01% after about 110 days (Fig. 4).

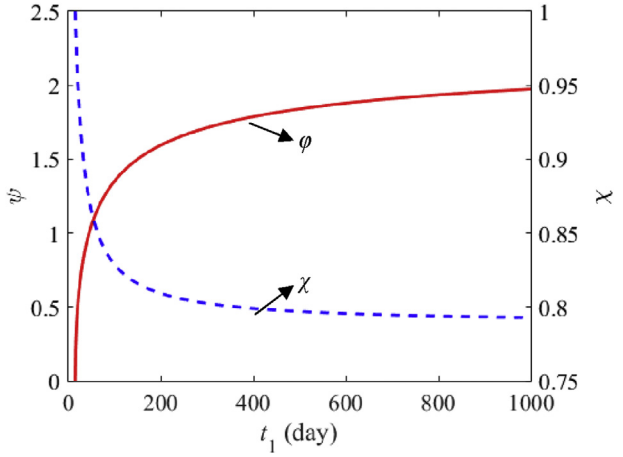

Fig. 3. Time-variation of creep coefficient φ and aging coefficient χ.

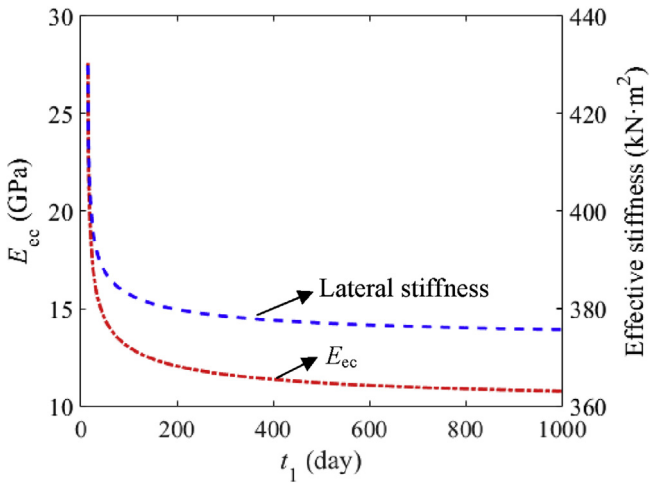

Fig. 4. Time-variation of age-adjusted effective modulus and effective lateral stiffness.

The lateral natural frequency ω and Euler buckling load P_{cr} of a CFST column are two parameters controlling the shapes of regions of dynamic instability of the column and they are also affected by the age-adjusted effective modulus E_{ec} or the effective lateral stiffness (E_sI_s + $E_{ec}I_c$) according to Eqs. (20) and (21). As shown in Fig. 5, due to the creep of the concrete core, the first lateral natural frequency ω_1 of the CFST column reduces rapidly from about 77.9 Hz to 73.6 Hz in 65

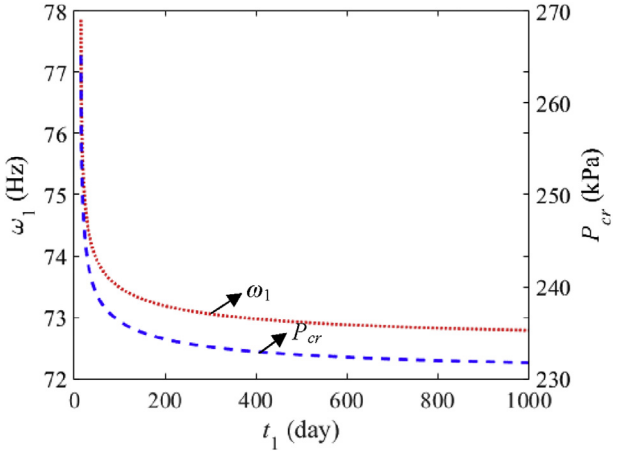

Fig. 5. Time-variation of natural frequency ω_1 and Euler buckling load P_{cr}.

days, and then slowly to 72.8 Hz in 1000 days. The natural frequency for each mode changes in a similar fashion. In addition, the Euler buckling load P_{cr} of the CFST column caused by the creep of the concrete core can reduce about 11.2% in the first 110 days and the reduction rate becomes less than 0.01% after the first 110 days as shown in Fig. 5. Therefore, in the investigation of the effects of the creep of the concrete core on the dynamic instability, it is proper to investigate the dynamic stability of CFST columns under the sustained central axial load when the periodic excitation is applied within 100 days after the first sustained loading time τ_0.

4.2.2. Time effect of concrete creep on dynamic instability region of CFST column

If the central axial periodic excitation is applied to the CFST column on any day of the first 5 days of the sustained static load, the corresponding boundaries of the principal region of dynamic instability on the plane (θ, P_t) are computed by the proposed method and shown in Fig. 6. In the computation, the sustained static load P_0 is assumed to be equal to $0.3P_{cr}$, i.e. the value of constant loading coefficient α is always set as $\alpha = P_0/P_{cr}(t_1) = 0.3$. That is, the possible dynamic instability is investigated when the static load is much smaller than the static instability load of the column.

It can be seen from Fig. 6 that the instability regions of the CFST column are significantly influenced by the time when the periodic excitation is applied. As the time of the application of the periodic excitation changes from the day τ_0 to the day τ_0+4, the instability region

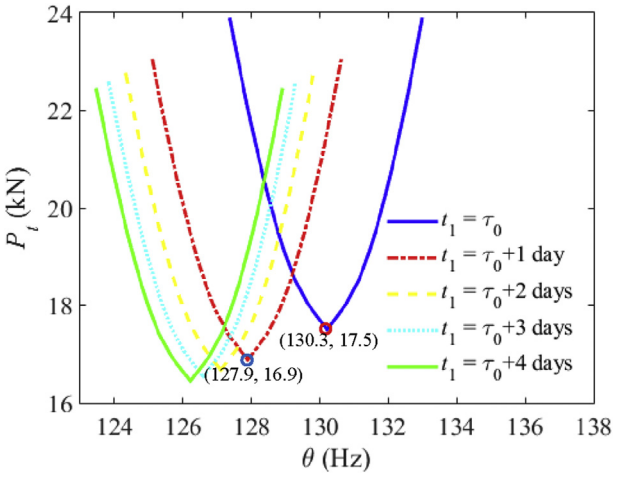

Fig. 6. Boundaries of instability regions of excitation applied at first 5 days after τ_0.

Table 2
Critical P_t and θ of excitation starting in 5 days after τ_0.

Time t_1 (day)	τ_0	τ_0+1	τ_0+2	τ_0+3	τ_0+4
Critical P_t (kN)	17.5	16.9	16.7	16.5	16.4
r_i for P_t (%)	–	3.4	1.2	1.2	0.6
θ (Hz)	130.3	127.9	127.1	126.6	126.2
r_i for θ (%)	–	1.8	0.6	0.4	0.3
P_{cr} (kN)	265	256	253	249	248

shifts towards the direction of lower frequencies θ and amplitudes P_t of the excitation. Hence, the column would become dynamically unstable under the excitation with smaller frequency and amplitude.

The values of the critical amplitude P_t and frequency θ when the excitation is applied in 5 days after the first static load at the time τ_0 are given in Table 2, in which the decreasing rate r_i = (value at day i - value at day i-1)/value at day i × 100%. Table 2 shows that the decreasing rates for critical P_t and θ gradually reduce when the column is periodically excited at the time of later days, and the total rates of decreasing of the critical P_t and θ are about 6% and 3% from the day τ_0 to the day τ_0+4. This indicates that the creep of the concrete core has significant effects on the critical amplitude P_t and frequency θ of the excitation for inducing dynamic instability of CFST columns.

In addition, because $\alpha = P_0/P_{cr}(t_1)$ and $P_{cr}(t_1)$ decreases with the time t_1 (Fig. 5 and Table 2), the constant value of the loading coefficient α actually means reducing the sustained static load P_0. Consequently, the values of the required sustained load, and the critical amplitude and frequency of the excitation for inducing dynamic instability all decrease if the excitation is applied at the time of later days. This means that the dynamic instability of the CFST column would occur under a smaller sustained central axial load owing to the creep of concrete.

Moreover, it is shown in Table 2 that the values of critical amplitude P_t of the excitation are only about 7% of the Euler critical load P_{cr}, so periodic excitation with amplitude much smaller than the static instability load could result in the dynamic instability of the CFST column.

4.2.3. Long-term time effect on the instability region

To further investigate the time effects of the creep of the concrete core on the boundaries of instability regions of the CFST columns, the boundaries of instability regions of the CFST column when the excitation is applied at the day τ_0 to the day (τ_0+105) are calculated by the proposed procedure and shown in Fig. 7. It is demonstrated that the region of dynamic instability shifts towards the direction of lower frequencies, and the shifting slows down when the excitation is applied after the day (τ_0+5). The critical amplitude P_t and frequency θ when

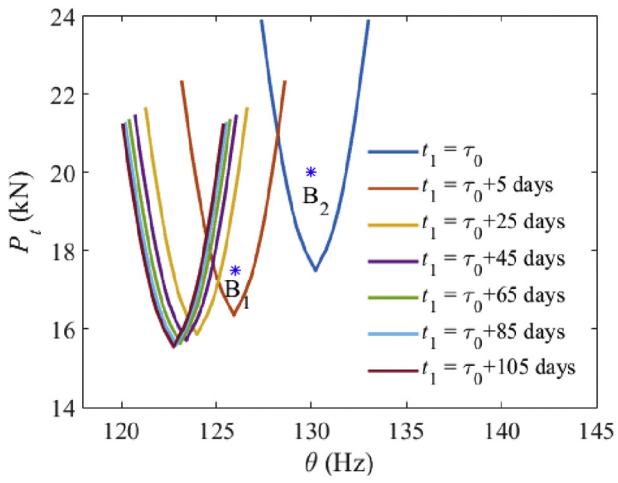

Fig. 7. Variation of boundaries of instability regions in about 100 days after τ_0.

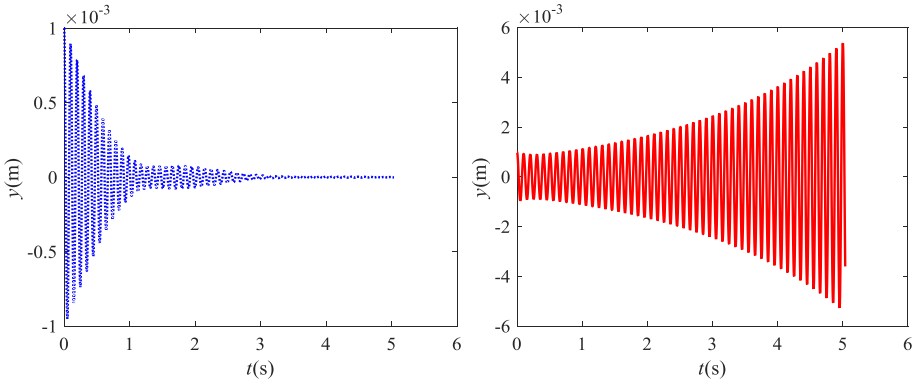

Fig. 8. Dynamic responses of point B_1 under different perturbance time (a) $t_1 = \tau_0$ day; (b) $t_1 = (\tau_0+5)$th day.

the excitation is applied at the day $t_1 = (\tau_0+105)$ are 15.6 kN and 122.7 Hz, respectively, which is equivalent to about 11% and 6% reduction of the critical value of P_t and θ in about 100 days and the reduction is about twice of that in the first 5 days.

For further manifesting the effect of concrete creep on the state of dynamic stability of the CFST column, two parametric points B_1 (130, 20) and B_2 (126, 17.5) are selected on the region plane of Fig. 7. Their modal responses $y(t)$ corresponding to the excitations applied at the day $t_1 = \tau_0$ and at the day $t_1 = (\tau_0+5)$ are given in Fig. 8 and Fig. 9, respectively. It can be observed that the dynamic state of the CFST column corresponding to point B_1 is stable at the day τ_0, i.e. the creep of the concrete core is insufficient to influence the lateral natural frequency and the lateral buckling load of the CFST column, while the point B_1 is located in the instability region when the excitation is applied at the time of the day (τ_0+5). However, the state of dynamics of the CFST column at the point B_2 changes from instability at the time τ_0 to stability when the excitation is applied at the time of the day (τ_0+5). Consequently, it is again demonstrated that the creep of concrete core could greatly influence the dynamic stability of CFST columns.

5. Conclusions

An analysis procedure for assessing the dynamic stability of slender CFST columns due to the time effects of the creep of the concrete core is proposed in this work based on the creep model of the ACI committee 209 and the effective modulus evaluation from the AEMM. Through the detailed numerical investigations on a typical CFST column, the validity and effectiveness of the proposed method is verified and the time-dependent characteristics of dynamic stability of the CFST column are explored.

For the typical CFST column under a sustained central axial load, its natural frequency and Euler buckling load decrease by about 5.5% and 11.2% in 65 days and 110 days, respectively. Since the natural frequency and Euler load are two key parameters directly influencing the regions of dynamic instability, and their absolute day rates of change become less than 0.01% in about 100 days, the time of 100 days of the creep of the concrete core can be used to evaluate the time effect of the creep of the concrete core on dynamic stability of the CFST column.

The dynamic stability of CFST column is significantly affected by the creep of the concrete core. Dynamic instability of a CFST column under a sustained central axial load much lower than its static lateral buckling load such as $P_0/P_{cr} = 0.3$ would occur in a few days when the creep of the concrete core shifts the amplitude and frequency of the excitation into the instability region of the column. With the development of creep, the CFST column would become dynamically unstable under a dynamic excitation with a very small amplitude P_t such as $P_t/P_0 = 2\%$. The critical amplitude P_t and frequency θ of the excitation can decrease by about 6% and 3% in 5 days of the first loading and respective 11% and 6% in 100 days. Under the same excitation, the dynamics of the CFST column could convert from stability to instability or changes in the opposite direction owing to the creep of the concrete core.

Acknowledgement

This work has been supported by the Chinese National Natural Science Foundation (51208126, 51608135) and the Technology Planning Project of Guangdong Province in China (2016B050501004).

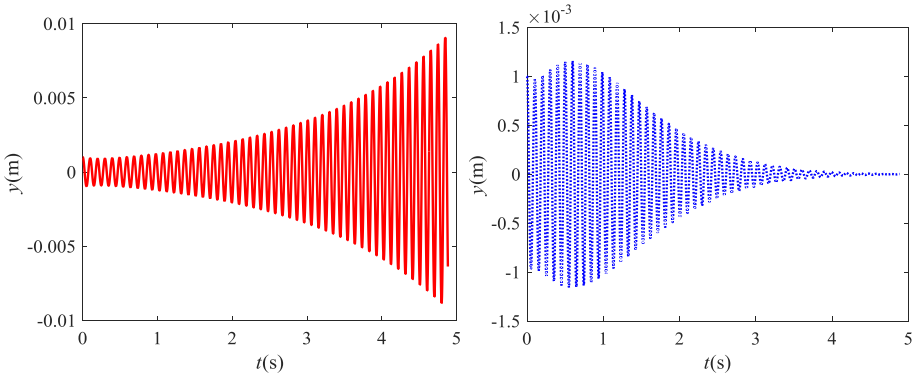

Fig. 9. Dynamic responses of point B_2 under different perturbance time (a) $t_1 = \tau_0$ day; (b) $t_1 = (\tau_0+5)$th day.

References

[1] Wu B, Wu D, Gao W, Song CM. Time-variant random interval response of concrete-filled steel tubular composite curved structures. Compos B Eng 2016;94:122–38.
[2] Wu D, Gao W, Feng J, Luo K. Structural behaviour evolution of composite steel-concrete curved structure with uncertain creep and shrinkage effects. Compos B Eng 2016;86:261–72.
[3] Han L, Li W, Bjorhovde R. Developments and advanced applications of concrete-filled steel tubular (CFST) structures: Members. J Constr Steel Res 2014;100:211–28.
[4] An Y, Han L, Zhao X. Behaviour and design calculations on very slender thin-walled CFST columns. Thin-Walled Struct 2012;53(2):161–75.
[5] Bazant ZP, Cedoliin L. Stability of structures: elastic, inelastic, fracture and damage theories. River Edge, USA: World Scientific; 2010.
[6] Schnabl S, Jelenić G, Planinc I. Analytical buckling of slender circular concrete-filled steel tubular columns with compliant interfaces. J Constr Steel Res 2015;115:252–62.
[7] Portolés JM, Romero ML, Filippou FC, Bonet JL. Simulation and design recommendations of eccentrically loaded slender concrete-filled tubular columns. Eng Struct 2011;33(5):1576–93.
[8] Dai X, Lam D, Jamaluddin N, Ye J. Numerical analysis of slender elliptical concrete filled columns under axial compression. Thin-Walled Struct 2014;77(4):26–35.
[9] Lahlou K, Lachemi M, Aïtcin PC. Confined high-strength concrete under dynamic compressive loading. J Struct Eng 1999;125(10):1100–8.
[10] Ge HB, Usami T. Cyclic tests of concrete-filled steel box columns. J Struct Eng 1996;122(122):1169–77.
[11] Nie JG, Wang YH, Fan JS. Experimental research on concrete filled steel tube columns under combined compression-bending-torsion cyclic load. Thin-Walled Struct 2013;67(2):1–14.
[12] Asadi H, Wang Q. Dynamic stability analysis of a pressurized FG-CNTRC cylindrical shell interacting with supersonic airflow. Compos B Eng 2017;118:15–25.
[13] Hazarika A, Mandal M, Maji TK. Dynamic mechanical analysis, biodegradability and thermal stability of wood polymer nanocomposites. Compos B Eng 2014;60:568–76.
[14] ACI 209 SP27-3. Prediction of creep, shrinkage and temperature effects in concrete structures. Designing for effects of creep, shrinkage and temperature in concrete structures. Detroit, MI. 1992. p. 51–93.
[15] Neville AM. Creep of concrete: plain, reinforced and prestressed. Amsterdam: North Holland Publishing Co.; 1970.
[16] Gilbert RI. Time effects in concrete structures. Amsterdam: Elsevier; 1988.
[17] Emara M, Torres L, Baena M, Bards C, Moawad M. Effect of sustained loading and environmental conditions on the creep behavior of an epoxy adhesive for concrete structures strengthened with CFRP laminates. Compos B Eng 2017;129:88–96.
[18] Gonilha JA, Correia JR, Branco FA. Creep response of GFRP-concrete hybrid structures: application to a footbridge prototype. Compos B Eng 2013;53:193–206.
[19] Choi KK, Meshgin P, Taha MMR. Shear creep of epoxy at the concrete-FRP interfaces. Compos B Eng 2007;38:772–80.
[20] Furlong RW. Strength of steel-encased concrete beam-columns. J Struct Division ASCE 1967;93:113–24.
[21] Uy B. Static long-term effects in short concrete-filled steel box columns under sustained loading. ACI Struct J 2017;98(1):96–104.
[22] Wang YY, Geng Y, Ranzi G, Zhang SM. Time-dependent behaviour of expansive concrete-filled steel tubular columns. J Constr Steel Res 2011;67(3):471–83.
[23] Han LH, Yang YF. Analysis of thin-walled steel RHS columns filled with concrete under long-term sustained loads. Thin-Walled Struct 2003;41(9):849–70.
[24] Naguib W, Mirmiran A. Creep modeling for concrete-filled steel tubes. J Constr Steel Res 2003;59(11):1327–44.
[25] Liu H, Wang YX, He MH, Shi YJ, Waisman H. Strength and ductility performance of concrete-filled steel tubular columns after long-term service loading. Eng Struct 2015;100:308–25.
[26] Ichinose LH, Watanabe E, Nakai H. An experimental study on creep of concrete filled steel pipes. J Constr Steel Res 2001;57(4):453–66.
[27] Bazant ZP. Prediction of concrete creep effects using age-adjusted effective modulus method. ACI J 1972;69:212–7.
[28] Luo K, Pi Y, Gao W, Bradford MA. Long-term structural analysis and stability assessment of three-pinned CFST arches accounting for geometric nonlinearity. Steel Compos Struct 2016;20(2):379–97.
[29] Neville AM, Dilger WH, Brooks JJ. Creep of plain and structural concrete. Longman Group Ltd: Construction Press; 1983.
[30] Bolotin VV. Dynamic stability of elastic systems (translation from the Russian). San Francisco, USA: Holden–Day Inc.; 1964.
[31] Farshad M. Stability of structures. Netherlands: Elsevier Science B.V.; 1994.
[32] Huang Y, Liu AR, Pi Y, Lu H, Gao W. Assessment of lateral dynamic instability of columns under an arbitrary periodic axial load owing to parametric resonance. J Sound Vib 2017;395:272–93.
[33] Huang Y, Lu H, Fu J, Liu A, Gu M. Dynamic stability of Euler beams under axial unsteady wind force. Math Probl Eng 2014:434868.
[34] Xie W. Dynamic stability of structures. New York: Cambridge University Press; 2006.
[35] Luo K, Pi Y, Gao W, Bradford MA, Hui D. Investigation into long-term behaviour and stability of concrete-filled steel tubular arches. J Constr Steel Res 2015;104:127–36.
[36] Li W, Han L, Chan TM. Performance of concrete-filled steel tubes subjected to eccentric tension. J Struct Eng ASCE 2015;141(12):04015049.
[37] Lee HP. Dynamic stability of spinning pre-twisted beams subject to axial pulsating loads. Comput Meth Appl Mech Eng 1995;127(1–4):115–26.
[38] Pi Y, Bradford MA, Qu W. Long-term non-linear behavior and buckling of shallow concrete-filled steel tubular arches. Int J Non Lin Mech 2011;46(9):1155–66.
[39] Riley W, Sturges L, Morris D. Mechanics of materials. sixth ed. Hoboken, USA: John Wiley & Sons Inc; 2007.
[40] Sahmani S, Ansari R, Gholami R, Darvizeh A. Dynamic stability analysis of functionally graded higher-order shear deformable microshells based on the modified couple stress elasticity theory. Compos B Eng 2013;51:44–53.
[41] Li C, Liu JJ, Cheng M, Fan XL. Nonlocal vibrations and stabilities in parametric resonance of axially moving viscoelastic piezoelectric nanoplate subjected to thermo-electro-mechanical forces. Compos B Eng 2017;116:153–69.
[42] Craig JrRR. Structural dynamics. New York, USA: John Wiley & Sons Inc; 1981.
[43] Liu A, Yang Z, Lu H, Fu J, Pi Y. Experimental and analytical investigation on the in-plane dynamic instability of arches owing to parametric resonance. J Vib Contr 2017. https://doi.org/10.1177/1077546317726210.
[44] Liu A, Lu H, Fu J, Pi Y, Huang Y, Li J, Ma Y. Analytical and experimental studies on out-of-plane dynamic instability of shallow circular arch based on parametric resonance. Nonlinear Dynam 2017;87:677–94.
[45] Tort C. Reliability-based performance-based design of rectangular concrete-filled steel tube (RCFT) members and frames Dissertation USA: The University of Minnesota; 2007